Synthesis and Structure of $Bi_{14}O_{20}(SO_4)$, A New Bismuth Oxide Sulfate

M. G. Francesconi, A. L. Kirbyshire, and C. Greaves*

School of Chemistry, University of Birmingham, Birmingham B15 2TT, U.K.

O. Richard and G. Van Tendeloo

EMAT, University of Antwerp (RUCA), Groenenborgerlaan 171, B-2020 Antwerp, Belgium

Received September 16, 1997. Revised Manuscript Received November 17, 1997

A new bismuth oxide sulfate of stoichiometry $Bi_{14}O_{20}(SO_4)$ has been synthesized from thermal treatment of an intimate mixture of α-Bi_2O_3 and $(NH_4)_2SO_4$ in the mole ratio 1:0.14, and its structure determined using a combination of electron diffraction, X-ray powder diffraction, and neutron powder diffraction. The body-centered tetragonal unit cell ($I4/m$; a = 8.664(1) Å, c = 17.282(2) Å) is a commensurate superstructure of the cubic fluorite subcell of δ-Bi_2O_3 (a_0): $a = (\sqrt{10}/2)a_0$, $c = 3a_0$. The structure contains discrete sulfate anions at the unit cell corners and body center, and a Bi−O framework of linked BiO_4e (e = lone pair of electrons) square pyramids and trigonal bipyramids. The square pyramids are aggregated into clusters of composition Bi_6O_8, comprising O^{2-} ions arranged in the form of a cube, the faces of which are capped by Bi^{3+} ions. In contrast, the trigonal bipyramids are corner linked to form layers perpendicular to [001]. The structure is thought to represent just one of several related phases in this system.

Introduction

The structural chemistry of bismuth(III) oxides and oxide fluorides is strongly influenced by stereochemically active $6(s/p)^2$ lone-pair electrons.[1] The Bi^{3+} ions are therefore generally located in low-symmetry sites, which may play important roles in the diverse and important properties of binary and ternary bismuth oxides, including ionic conductors (e.g., δ-Bi_2O_3),[2] catalysts (e.g., Bi_2MoO_6),[3] ferroelectrics (e.g., Bi_2MoO_6)[4] and high-temperature superconductors (e.g., $Bi_2Sr_2CaCu_2O_8$).[5] In this paper, we report the synthesis of a new bismuth oxide phase, which contains a small amount of SO_4^{2-} ions. The structure is related to that of δ-Bi_2O_3, with the SO_4^{2-} ions located at Bi sites, but ordered to produce a new structure containing $Bi_6O_8^{2+}$ clusters.

δ-Bi_2O_3 is the best oxide ionic conductor at elevated temperatures, with a conductivity of ∼1 Ω^{-1} cm^{-1} at 750 °C.[2] It has a fluorite (face-centered cubic) structure, such that in the absence of oxygen vacancies, cubic BiO_8 polyhedra would be present. However, the oxygen sublattice is 25% deficient with the vacancies highly disordered, although neutron diffraction has suggested short-range order consistent with a preference for two vacancies to be oriented in a ⟨111⟩ configuration around Bi.[6] Calculations[7] have suggested the presence of both ⟨111⟩ and ⟨110⟩ defects, and the high degree of structural disorder plays a major role in the conductivity mechanism.

Unfortunately, the δ-phase is a high-temperature form of Bi_2O_3 and is stable only between 664 °C and the melting point of Bi_2O_3, 824 °C. On cooling, two metastable phases may occur, i.e., the tetragonal β-phase at 650 °C and the body-centered cubic γ phase at 639 °C. These phases transform into the α-phase in the temperature range 600−500 °C.[8] The δ-phase can be stabilized at room temperature by doping Bi_2O_3 with either isovalent (e.g., Y^{3+}) or aliovalent (e.g., Ba^{2+}) cations,[2] but such substitutions result in lower conductivities.[2]

Several bismuth oxide−sulfate phases have been prepared from the pyrolysis of $Bi_2(SO_4)_3$. $Bi_2O_2SO_4$ has been reported to be the first product,[9,10] and subsequent pyrolysis results in additional loss of SO_3 to form two different phases with compositions $Bi_2O_3{\cdot}0.9SO_3$ [$Bi_{26}O_{27}(SO_4)_{12}$] and $Bi_2O_3{\cdot}0.67SO_3$ [$Bi_{14}O_{16}(SO_4)_5$].[11] Both contain free SO_4^{2-} ions and fluorite-related regions: Bi_2O_2-like regions in the former and isolated $Bi_{14}O_{16}^{10+}$ blocks infinitely extended along the b direction in the latter. $Bi_2O_3{\cdot}0.9SO_3$ and $Bi_2O_3{\cdot}0.67SO_3$ are characterized by a lower SO_3 content compared to the parent compound $Bi_2O_2SO_4$, and the loss of SO_3 causes structural changes

(1) Andersson, S.; Åström, A. NBS Spec. Pub. 364; *Solid State Chem.* **1972**, 3.
(2) Takahashi, T.; Iwahara, H. *Mater. Res. Bull.* **1978**, *13*, 1447.
(3) Schuit, G. C. A. *J. Less Common Met.* **1974**, *36*, 329.
(4) Theobald, F.; Laarif, A.; Hewat, A. W. *Ferroelectrics* **1984**, *56*, 219.
(5) Maeda, M.; Tanaka, Y.; Fukukumi, M.; Asaro, Q. T. *Jpn. J. Appl. Phys.* **1988**, *27*, L209.
(6) Battle, P. D.; Catlow, C. R. A.; Drennan, J.; Murray, A. D. *J. Phys. C* **1983**, *16*, L561.
(7) Jacobs, P. W. M., MacDonaill, D. A. *Solid State Ionics* **1987**, *23*, 279.
(8) Harwig, H. G.; Gerards, A. G. *Thermochim. Acta* **1979**, *28*, 21.
(9) Matsuzaki, R.; Sofue, A.; Masumiza, H.; Sack, Y. *Chem. Lett.* **1974**, *4*, 737.
(10) Margulis, E. V.; Grishankina, N. S.; Kopylov, N. I. *Russ. J. Inorg. Chem.* **1965**, *10*, 1253.
(11) Aurivillius, S. *Acta Chem. Scand. A* **1987**, *41*, 415.

S0897-4756(97)00625-X CCC: $15.00
Published on Web 01/21/1998

as the Bi_2O_2 layers progressively change to CaF_2-like blocks.

Given the stabilization of the γ-Bi_2O_3 structure (sillenite) by small amounts of tetrahedral ions, e.g., $Bi_{12}SiO_{20}$, $Bi_{12}GeO_{20}$ [for example, ref 12], it seemed pertinent to explore the possibility of introducing lower concentrations of SO_4^{2-} ions into Bi_2O_3 and examine the structural consequences. To achieve better control and reproducibility of the SO_4^{2-} stoichiometry in the final product, we have examined a different synthetic strategy based on the use of Bi_2O_3 and $(NH_4)_2SO_4$ as starting reagents for the formation of Bi oxide sulfates. In this way we have achieved precise stoichiometry control and here report the synthesis and structural characterization of a new bismuth oxide sulfate with reduced sulfate concentration.

Experimental Section

Stoichiometric amounts of high-purity Bi_2O_3 and $(NH_4)_2SO_4$ were intimately mixed together and were subjected to an initial low-temperature treatment at 225 °C for 3 h to allow the decomposition of $(NH_4)_2SO_4$ and its chemisorption on the surface of the Bi_2O_3 particles. Subsequently the samples underwent a higher temperature treatment at 750 °C for 10 h to promote the solid-state reaction:

$$Bi_2O_3 + x(NH_4)_2SO_4 \rightarrow Bi_2O_{3-x}(SO_4)_x + 2xNH_3 + xH_2O \qquad (0.1 < x < 0.2)$$

The structures of the samples were examined by X-ray powder diffraction (XRD; Siemens D5000, primary beam monochromator, transmission mode, with position-sensitive detector). An electron diffraction study was performed on a monophasic sample ($x = 0.14$) using a Philips CM20 microscope operating at 200 kV.

Structure refinement of this sample was achieved at ambient temperature using both X-ray and time-of-flight neutron powder diffraction data, the latter collected from the LAD diffractometer, Rutherford Appleton Laboratory. The refinement programs Fullprof[13] and TF12LS, based on the Cambridge Crystallography Subroutine Library,[14,15] were used for X-ray and neutron refinements, respectively.

Given the possibility that some sulfate (SO_3) may be lost during synthesis, the sulfate content of the single-phase sample was determined using ICP emission spectroscopy. The determined SO_4 content (2.78%) was in excellent agreement with that initially weighed out (2.82%) and confirmed that the synthetic strategy adopted provides precise stoichiometry control.

Results and Discussion

Insertion/substitution of anions in an oxide structure can be achieved by solid-state reaction using appropriate agents. Ammonium salts are particularly suitable due to the low-temperature volatility of the ammonium cationic group, which allows only the anion to react with the oxide. In contrast to previous research involving the use of ammonium fluoride in a one-stage low-temperature reaction,[16] in the present case a two-stage synthesis was employed to minimize the risk of anion loss through volatilisation. In the first stage (225 °C for 3 h) only the decomposition of $(NH_4)_2SO_4$ and chemisorption of the decomposed product on Bi_2O_3 grains surfaces is promoted and no reaction with the oxide bulk is indicated in XRD traces; to take the $(SO_4)^{2-}$ insertion to completeness, a higher temperature stage is necessary (750 °C for 10 h).

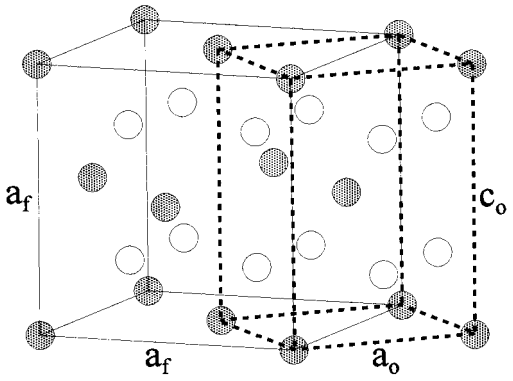

Figure 1. Fluorite unit cell showing its relationship to the small tetragonal subcell found for $Bi_2O_{3-x}(SO_4)_x$, $x = 0.14$. Cations and anions are shaded and open circles, respectively.

Single-phase samples of the $Bi_2O_{3-x}(SO_4)_x$ series were obtained in the narrow composition range $0.13 < x < 0.16$; for $x < 0.13$ the XRD pattern showed peaks of unreacted Bi_2O_3, and for $x > 0.16$ extra peaks were observed which appeared to indicate another phase in the Bi−O−SO_4 system. A more detailed examination of the phase diagram is currently in progress in order to determine the nature of this phase and others observed at even higher sulfate levels. A sample with $x = 0.14$ was chosen for further examination, and XRD data showed several intense peaks and a large number of additional weak peaks. The intense reflections were consistent with a body-centered tetragonal unit cell (subcell $a_0 = 3.875(1)$, $c_0 = 5.760(2)$ Å), which is related to the cubic fluorite cell, edge a_f, by $a_0 = a_f/\sqrt{2}$, $c_0 = a_f$; see Figure 1.

The electron microdiffraction technique allowed us to construct the reciprocal lattice and therefore the direct lattice. The $[001]_{subcell}$ and $\langle 100 \rangle_{subcell}$ electron microdiffraction zone axis patterns (Figure 2) contained fundamental and superlattice reflections and furthermore first-order Laue zone reflections. By taking into account the position of these reflections with regard to the position of the zero-order Laue zone reflections and by considering the radii of the high-order Laue zones, the reciprocal lattice was constructed (Figure 3). From the reciprocal lattice which is face-centered tetragonal, the body-centered tetragonal direct lattice with lattice parameters $a = \sqrt{5}a_0$ ($=(\sqrt{10}/2)a_f$), $c = 3c_0$ ($=3a_f$) was inferred. All the obtained electron microdiffraction patterns and all the weak peaks in the XRD pattern could be indexed on such a cell, confirming that the sample is indeed single phase.

The space group was determined in a two-step procedure. Initially, the partial extinction symbol was

(12) Radaev, S. F.; Simonov, V. I.; Kargin, Y. F. *Acta Crystallogr. B* **1992**, *48*, 604.
(13) Fullprof, v3.2, 1997, Rodriguez-Carvajal, J., based on the original code by Wiles, D. B., Young, R. A., Sakthivel, A. *J. Appl. Crystallogr.* **1981**, *14*, 149.
(14) Matthewman, J. C.; Thompson, P.; Brown, P. J. *J. Appl. Crystallogr.* **1982**, *15*, 167.
(15) Brown, P. J.; Matthewman, J. C. Rutherford Appleton Laboratory Report RAL-87-010, 1987.
(16) Slater, P. R.; Edwards, P. P.; Greaves, C.; Gameson, I.; Francesconi, M. G.; Hodges, J. P.; Al-Mamouri, M.; Slaski, M. *Physica C* **1995**, *241*, 151.

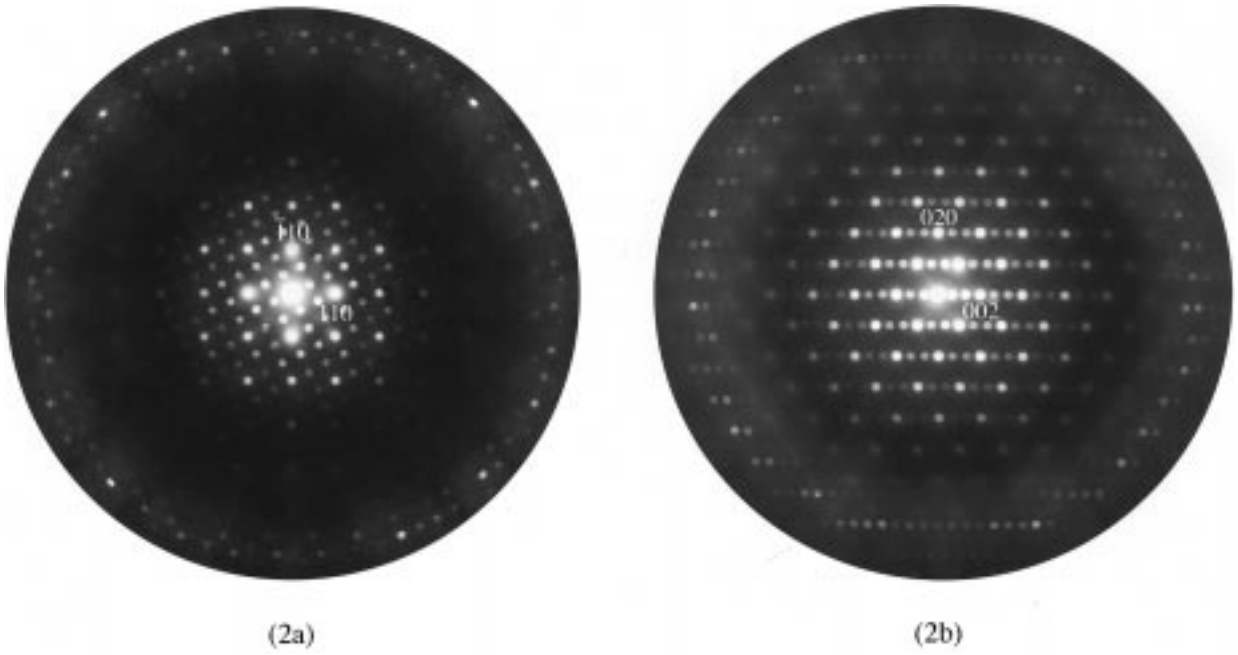

Figure 2. (a) $[001]_{subcell}$ electron microdifffraction pattern. (b)$\langle 100\rangle_{subcell}$ electron microdiffraction pattern. These patterns are indexed with the subcell lattice.

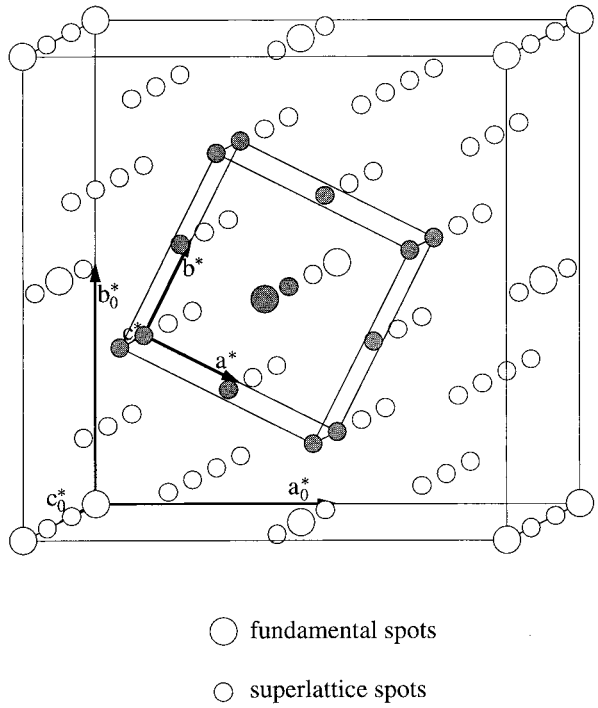

Figure 3. Reciprocal lattice of $Bi_2O_{3-x}(SO_4)_x$, $x = 0.14$.

obtained by observing the zero- and first-order Laue zone of characteristic electron microdiffraction patterns (depending on the crystal system) and by comparing them with simulations.[17] This symbol was consistent with a few space groups belonging to different point groups. The point group was then determined from information in convergent beam electron diffraction (CBED) patterns.[18,19] For the tetragonal crystal system, the determination of the partial extinction symbol required the analysis of the [001], ⟨100⟩, and ⟨110⟩ zone axis patterns.[17]

On the [001] zone axis pattern (Figure 4), the zero-order Laue zone reflections form a noncentered square. In the first-order Laue zone, the reflections also form a noncentered square with the same size. This is characteristic of the absence of a glide plane perpendicular to the zone axis. Moreover, there was no first-order Laue zone reflection on two of the four "net" mirrors (the "net" symmetry takes into account only the position of the reflections and not their intensity). The simulation corresponding to this experimental pattern is presented in Figure 4, and the individual partial extinction symbol is I−••.

By performing the same analysis on the [100] and [110] zone axis patterns, the partial extinction symbols I•−• and I••− were inferred, respectively. It is worth noting that since the first-order Laue zone reflections were absent from well-oriented patterns, the electron beam was slightly tilted along the zero-order Laue zone "net" mirrors in order to observe them. The partial extinction symbol I− − − was obtained by adding the three symbols previously determined.

According to the *International Tables for Crystallography*,[20] this symbol is in agreement with 10 space groups belonging to 8 different point groups, as shown in Table 1. The "ideal" symmetry (which takes into account both position and intensity of the reflections) of the [001] CBED zone axis pattern presented in Figure 5a is (*4*). This symmetry is consistent, according to Table 2,[17] with the 4/*m*, 4, and $\bar{4}$ point groups. To determine unambiguously the point group, the [131] CBED zone axis pattern was observed (Figure 5b). The zero-order Laue zone "ideal" symmetry is (*2*), which agrees with the 4/*m* and 4/*mmm* point groups. The only

(17) Morniroli, J. P.; Steeds, J. W. *Ultramicroscopy* **1992**, *45*, 219.
(18) Buxton, B. F.; Eades, J. A.; Steeds, J. W.; Rackham, G. M. *Proc. R. Soc. (London) A* **1976**, *281*, 171.
(19) Tanaka, M.; Saito, R.; Sekii, H. *Acta Crystallogr. A* **1983**, *39*, 357.
(20) *International Tables for Crystallography*; Hahn, T., Ed.; Reidel: Dordrecht, 1992.

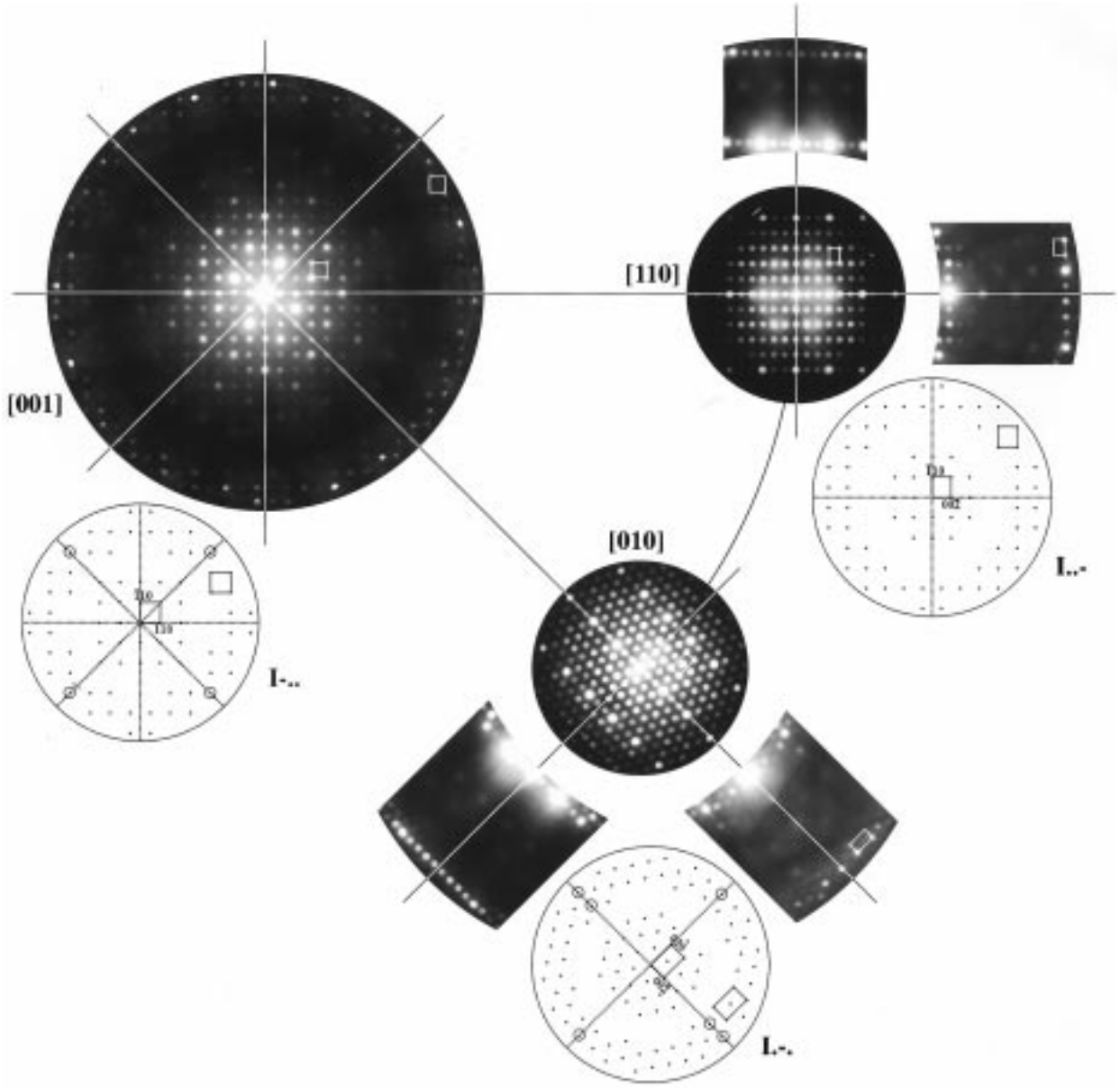

Figure 4. [001], [100], and [110] zone axis electron microdiffraction patterns and corresponding theoretical patterns.

Table 1. Space Groups Belonging to the Tetragonal Crystal System in Agreement with the I− − − Partial Extinction Symbol[19]

point group	4	$\bar{4}$	4/*m*	422	4*mm*	$\bar{4}$2*m*	$\bar{4}$*m*2	4/*mmm*
space group	*I*4 *I*41	*I*$\bar{4}$	*I*4/*m*	*I*422 *I*4122	*I*4*mm*	*I*$\bar{4}$2*m*	*I*$\bar{4}$*m*2	*I*4/*mmm*

compatible point group is therefore 4/*m*, and the space group is *I*4/*m*.

Due to the large unit cell, structure refinement involved two steps. The nature of the Bi sublattice, especially the question of whether SO_4 groups were substituted at Bi positions, was first investigated using Rietveld methods and XRD data, which are only marginally influenced by scattering from the O^{2-} ions. This was followed by determination of the O sublattice using neutron powder diffraction data. For the initial model for XRD refinement, approximate atomic coordinates in the supercell were estimated from the above-mentioned structural relationship with the tetragonal subcell. The refinement confirmed the space group *I*4/*m* with $(SO_4)^{2-}$ anions located on the Bi^{3+} sites at the origin and body center. The unit cell therefore contains $28Bi^{3+}$ ions and $2(SO_4)^{2-}$ ions, corresponding to $2Bi:0.143(SO_4)$ and in excellent agreement with the ratio present in the starting reagents. Since the XRD profile is determined largely by the Bi^{3+} cations, no attempt was made to refine the oxygen positions or occupancies, which were constrained at their ideal values for a simple fluorite-type δ-Bi_2O_3 structure. However, a single overall isotropic temperature factor was refined for the O sites, and all the refined structural parameters are listed in Table 3. As expected, the inadequacy of the O sublattice is reflected in the high O temperature factor. The observed and calculated profiles are shown in Figure 6.

Since the XRD data are dominated by scattering from the Bi^{3+} ions, the refined Bi positions from the XRD refinement were assumed to be accurate despite the errors relating to the O^{2-} sites and were therefore used to provide a reliable data set for examination of the O sublattice using the neutron diffraction data. By initially constraining the Bi positions to accord with the XRD refinement, the essential features of the O^{2-}

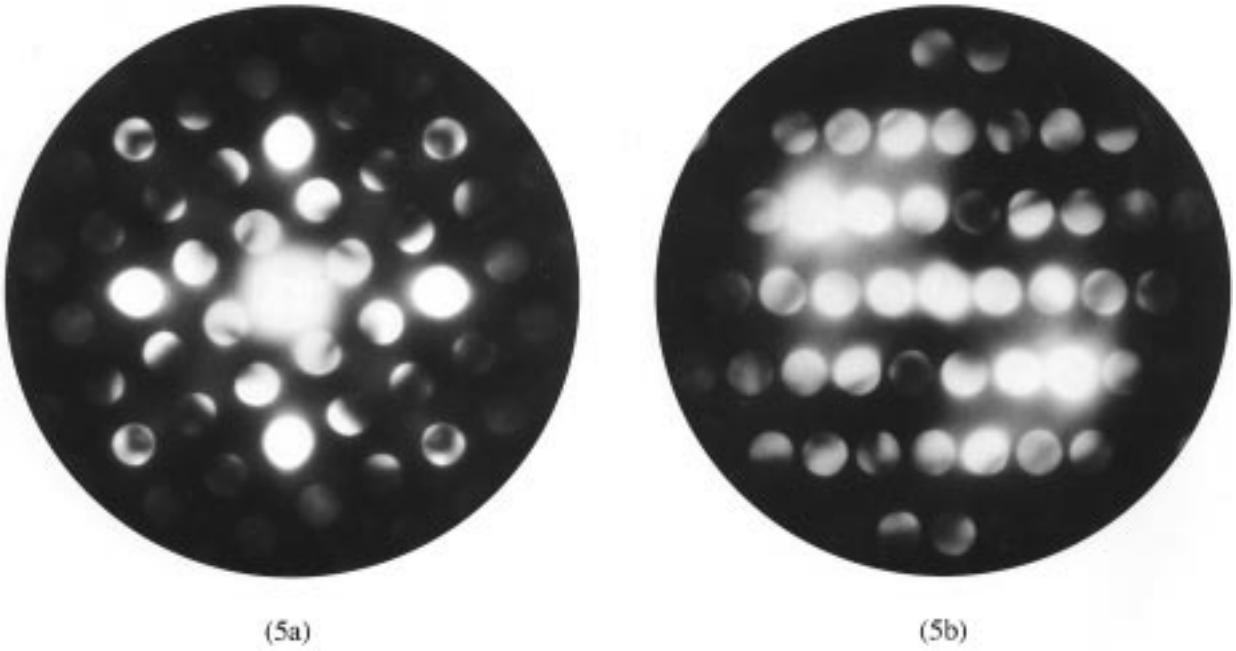

(5a) (5b)

Figure 5. (a) [001] CBED pattern. (b) [131] CBED pattern.

Table 2. Zero-Order Laue Zone "Ideal" Symmetry of the Different Zone Axis Patterns for the Different Point Groups Belonging to the Tetragonal Crystal System[17]

tetragonal	[001]	⟨100⟩	⟨110⟩	[uv0]	[u0w]	[uuw]	[uvw]
$\frac{4}{m}mm$	(4*mm*)	(2*mm*)	(2*mm*)	(2*mm*)	(2*mm*)	(2*mm*)	(2)
$\bar{4}2m$	(4*mm*)	(2*mm*)	(*m*)	(*m*)	(*m*)	(*m*)	(1)
4*mm*	(4*mm*)	(*m*)	(*m*)	(*m*)	(*m*)	(*m*)	(1)
422	(4*mm*)	(2*mm*)	(2*mm*)	(*m*)	(*m*)	(*m*)	(1)
$\frac{4}{m}$	(4)			(2*mm*)			(2)
$\bar{4}$	(4)			(*m*)			(1)
4	(4)			(*m*)			(1)

Table 3. Refined Atomic Parameters (X-ray Diffraction)[a]

ions	position	*x*	*y*	*z*	*B*/Å^2	cell occupancy
S	2a	0	0	0	0.96(4)	2
Bi1	8h	0.2147(5)	0.4390(4)	0	0.96(4)	8
Bi2	16i	0.2982(4)	0.1050(3)	0.1696(2)	0.96(4)	16
Bi3	4e	0.5	0.5	0.1585(3)	0.96(4)	4
O1	8g	0.5	0	0.0833	7.7(6)	6
O2	16i	0.1	0.2	0.25	7.7(6)	12
O3	16i	0.3	0.6	0.0833	7.7(6)	12
O4	4d	0.5	0	0.25	7.7(6)	3
O5	16i	0.1	0.2	0.083	7.7(6)	12

[a] $a = b = 8.664(1)$ Å, $c = 17.282(2)$ Å. $R_{wp} = 14.5\%$, $R_E = 3.5\%$, $R_I = 9.4\%$.

sublattice immediately became apparent: the O4 and O5 sites (Table 3) are empty, whereas O1, O2, and O3 are fully occupied. There are thus 40 O^{2-} ions per unit cell and 20 vacancies arranged in a completely ordered fashion to give unit cell contents of $Bi_{28}O_{40}(SO_4)_2$. Approximate positions of the O atoms of the SO_4^{2-} groups were also located, with two being in the $z = 0$ plane and two above and below the S atom, slightly displaced off the [001] axis. The refined atomic parameters are shown in Table 4, and selected bond distances and angles are listed in Table 5. Observed, calculated, and difference neutron diffraction profiles are shown in Figure 7, and the structure is illustrated in Figure 8, projected along [010]. The very small unfitted peak at $d \sim 2.7$ Å is attributed to minor contamination with a phase of higher sulfate concentration, which is currently being investigated.

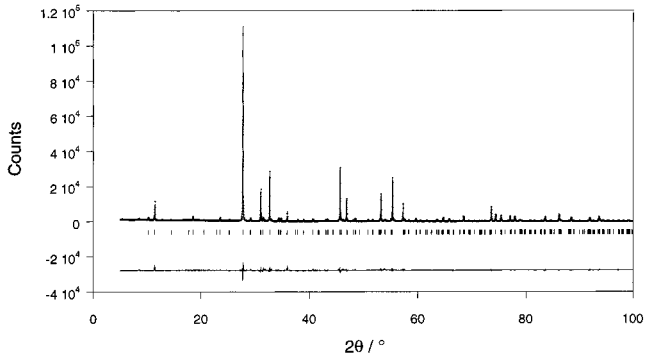

Figure 6. Observed (+) calculated and difference XRD profiles for $Bi_2O_{3-x}(SO_4)_x$, $x = 0.14$; the reflection positions are marked by vertical lines.

Table 4. Refined Atomic Parameters (Neutron Diffraction)[a]

ions	position	*x*	*y*	*z*	*B*/Å^2	cell occupancy
S	2a	0	0	0	0.96(3)	2
Bi1	8h	0.2124(7)	0.4366(5)	0	0.96(3)	8
Bi2	16i	0.2973(6)	0.1057(5)	0.1691(2)	0.96(3)	16
Bi3	4e	0.5	0.5	0.1579(4)	0.96(3)	4
O1	8g	0.5	0	0.1245(6)	1.21(5)	8
O2	16i	0.0742(6)	0.2509(7)	0.2565(3)	1.21(5)	16
O3	16i	0.3181(7)	0.6218(7)	0.0799(4)	1.21(5)	16
O4[b]	8h	0.011(4)	0.172(4)	0	8.7(8)	4
O5[b]	16i	0.036(3)	0.036(3)	0.084(2)	8.7(8)	4

[a] $a = b = 8.660(1)$ Å, $c = 17.272(2)$ Å. $R_{wp} = 5.14\%$, $R_E = 0.68\%$, $R_I = 6.14\%$. [b] O4 and O5 are bonded to S.

The structure shows that the Bi^{3+} ions are 4-coordinate with stereochemically active lone pairs of electrons, BiO_4e: Bi1 and Bi3 are characterized by square-pyramidal coordination, while Bi2 is trigonal bipyramidal (Figure 9). Whereas the trigonal bipyramidal Bi^{3+} polyhedra are linked to form layers perpendicular to [001], Bi1 and Bi3 form discrete clusters of stoichiometry Bi_6O_8, in which the O atoms describe a cube, the faces of which are capped by Bi. Interestingly, this cluster is a structural element within the basic fluorite

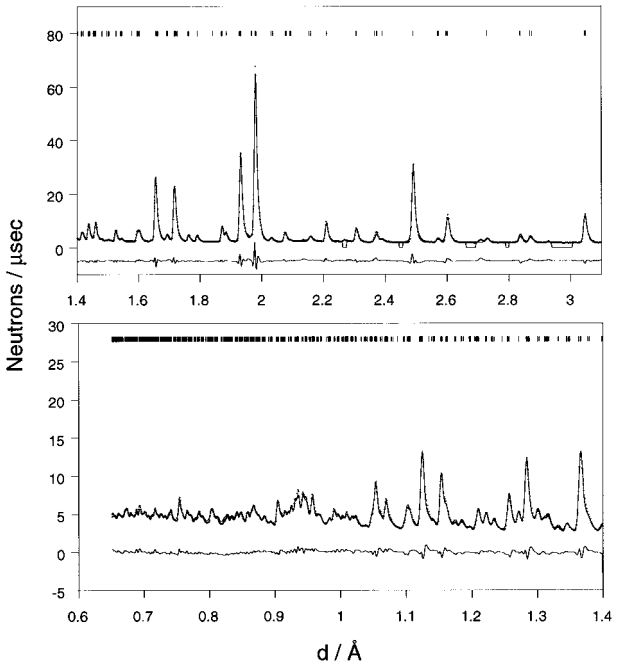

Figure 7. Reflection positions and the observed (+), calculated and difference neutron diffraction profiles for $Bi_{14}O_{20}(SO_4)$. Since refinement was performed only over regions where reflections contribute, some regions have calculated and difference profiles set to zero.

Table 5. Selected Bond Distances (Å) and Angles (deg)

S−O4	1.49(2) [×2]	Bi1−O2	2.305(7) [×2]
S−O5	1.52(3) [×2]		2.241(7) [×2]
O4−S−O4	90	O2−Bi1−O2	72.3(2) [×2]
O5−S−O5	146.4(1.6)		73.6(2)
			76.1(2)
			115.6(2) [×2]
Bi2−O1	2.125(6)	Bi3−O2	2.325(6) [×4]
Bi2−O2	2.500(8)		
Bi2−O3	2.207(7)	O2−Bi3−O2	70.4(2) [×4]
Bi2−O3	2.104(7)		109.2(2) [×2]
O1−Bi2−O2	82.0(2)		
O1−Bi2−O3	95.4(2)		
	92.2(2)		
O2−Bi2−O3	78.1(2)		
	173.0(3)		
O3−Bi2−O3	95.5(2)		

structure. $Bi_{14}O_{20}(SO_4)$ therefore has an oxygen sublattice which displays complete order, with all sites having occupancies of zero or one. In this respect, it differs markedly from the structure of δ-Bi_2O_3, where 75% of the oxygen sites in the fluorite structure are occupied randomly, and the disorder in the anion sublattice promotes a mechanism of hopping of the oxygen ions which is responsible for the high ionic conductivity of this phase.

The O atoms of the SO_4^{2-} groups have very high isotropic thermal parameters (9 Å^2, Table 4), which implies that the true arrangement of these groups may not be satisfactorily represented by the proposed model. Although the S−O bond distances (1.49 and 1.52 Å, Table 5) are typical for sulfate anions (e.g., S−O 1.48 Å in Na_2SO_4),[21] the O−S−O angles correspond to severe distortion from the ideal tetrahedral symmetry. Although the O4 and O5 sites bonded to S are only

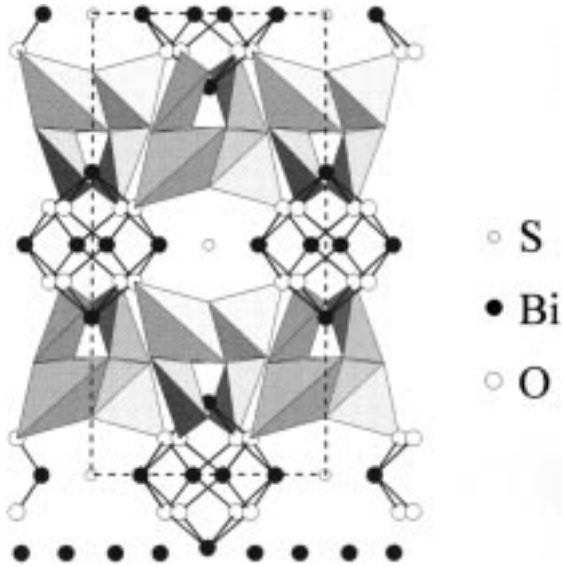

Figure 8. Structure of $Bi_{14}O_{20}(SO_4)$ projected along [010]. The Bi−O bonds of the BiO_4e square pyramids are marked, and the BiO_4e trigonal bipyramids are shown as solid polyhedra. The oxygens of the $(SO_4)^{2-}$ groups are not shown.

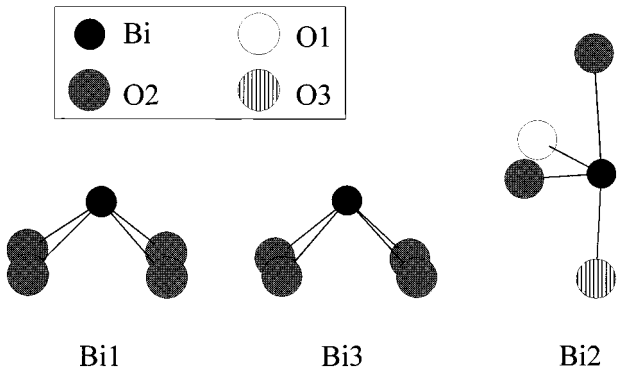

Figure 9. Coordination around Bi^{3+} at the Bi1, Bi2, and Bi3 positions.

partially occupied, the space group requires the angle O4−S−O4 to be 90° if S is positioned at the origin. It is possible that rotational oscillation of the SO_4^{2-} groups may contribute to the magnitude of the temperature factor. Higher resolution neutron diffraction data are required in order to clarify the structural nature of these groups.

The structure is particularly interesting since it contains Bi^{3+} ions in both of its preferred stereochemistries: square pyramidal (Bi1 and Bi3) and trigonal bipyramidal with an equatorial lone pair (Bi2). The O configurations around Bi1 and Bi3 (Table 5) are very similar to those found in materials with $Bi_2O_2^{2+}$ layers: in BiOCl, for example, the Bi−O bond is 2.316 Å and O−Bi−O angles are 72.8°.[22] Also, the BiO_4e coordination around Bi2 resembles that found in α-Bi_2O_3[23] and β-Bi_2O_3.[24] In all cases, the Bi−O equatorial bonds are approximately 2.1 Å and are shorter than the axial bonds (2.21 and 2.50 Å for Bi2 in this study; 2.2−2.3 and 2.5−2.6 Å for the two Bi^{3+} ions in α-Bi_2O_3;[23]

(21) Nord, A. G. *Acta Chem. Scand.* **1973**, *27*, 814.

(22) Keramidas, K. G.; Voutsas, G. P.; Rentzeperis, P. I. *Z. Kristallogr.* **1993**, *205*, 35.

(23) Aurivillius, B.; Malmros, G. *K. Tekn. Högsk. Handl.* **1972**, *291*, 544.

(24) Blower, S. K.; Greaves, C. *Acta Crystallogr. C* **1988**, *44*, 587.

2.3 and 2.5 Å in β-Bi_2O_3[24]). The equatorial and axial O−Bi2−O angles (78.1°/173°) also compare favorable with those in α-Bi_2O_3 (93°/159° and 78°/170°)[23] and β-Bi_2O_3 (82°/172°).[24] The reduction of the equatorial angle below the ideal (120°) and the lengthening of the axial bonds can be attributed to electron repulsion effects associated with the lone pair of electrons on the Bi^{3+}.

Conclusions

A route has been found that allows the synthesis of bismuth oxide sulfates with accurately controlled stoichiometry; it is possible that the procedure can be adapted to other metals, and hence it offers potential for the synthesis of a wide range of new metal oxide sulfates. The new Bi(III) oxide sulfate $Bi_{14}O_{20}(SO_4)$ has been characterized structurally, and the sulfate groups are centered on cation positions in a structure that can be related to the defect fluorite structure of δ-Bi_2O_3. SO_4 groups periodically replace Bi^{3+} ions and their first O^{2-} coordination shells to provide a large commensurate superstructure with a unit cell 7.5 times larger than the fluorite subcell. The incorporation of the oxyanion groups produces complete ordering of the oxygen sublattice to give Bi^{3+} ions with coordinations (square pyramidal and trigonal bipyramidal) indicative of stereochemically active $6(s/p)^2$ lone pairs of electrons. To our knowledge, this material is the first example of Bi^{3+} exhibiting both of these favored stereochemistries in the same compound.

Acknowledgment. We thank EPSRC for financial support and for the provision of neutron diffraction facilities. We are grateful to S. Hull for experimental assistance with the collection of neutron diffraction data.

CM9706255